DETERMINATION OF THE PRE-LAUNCH IMAGE-PROCESSING TECHNIQUES FOR LIQUID CRYSTAL TUNABLE FILTER (LCTF) FOR PHL-MICROSAT DIWATA-1

Maestro, M. M.[1], Paringit, E. C.[1], Viray, F. M.[1], Calvo, J. S.[1], Ishida, T.[2],
Takahashi, Y.[2], Kurihara, J.[2], Vergel, K.[2], Magallon, B. P[2].

[1]University of the Philippines Training Center for Applied Geodesy and Photogrammetry
Diliman, Quezon City, Metro Manila, Philippines
[2]Hokkaido University
Kita Ward,Sapporo, Hokkaido Prefecture 060-0808, Japan

alainmmaestro@gmail.com

KEY WORDS: remote sensing, image processing, DIWATA, PHL-Microsat, microsatellite

ABSTRACT: The Program, "Development of Philippine Scientific Earth Observation Microsatellite (PHL-MICROSAT) has successfully launched a microsatellite called Philippines' first microsatellite, DIWATA-1 last April 2016. DIWATA-1 is equipped with remote sensing sensors. It seeks to maximize and utilize its earth observation capabilities as applied in resource and disaster management and weather observations in the Philippines through multispectral images taken by its cameras. One of the payloads mounted in the microsatellite is the Space-borne Multi-spectral Imager (SMI) with Liquid Crystal Tunable Filter (LCTF), specifically made and designed for DIWATA-1. Like any other optical imaging sensors, it contains radiometric noise and geometric distortions and images should be further projected unto a map coordinate system. Thus, a methodology to increase the radiometric precision and to correct geometric distortions of DIWATA-1's images is necessary. This research used data from laboratory and practical airborne experiments of an LCTF Camera to design the image-processing line. Corrections introduced include radiance offsets, and reduction of transmittance limitation and vignetting caused by the camera's optical assembly composed of a charge-coupled device (CCD), filter and lenses. An irradiance model was adapted to account for radiometric corrections due to viewing, terrain and sun-angle conditions. Processed LCTF and DIWATA-1 geospatial images will give way to level 1 satellite products which can be used or further processed by government agencies and research institutions for different applications.

INTRODUCTION

1. Background

Philippines belongs to the most disaster-prone countries in the world ranking from 4th to 3rd according to the United Nations Office for Disaster Risk Reduction (UNISDR) Report in 2015 and 2016. It is also one of the 18 mega-biodiverse countries of the world, containing two-thirds of the earth's biodiversity and between 70% and 80% of the world's plant and animal species. The majority of the country's workforce belongs to the agriculture sector. The Philippine Government has been spending multi-million pesos to purchase imageries from commercial providers in aid of the country's needs. In Year 2015, recognizing the advantages of having and using its own satellite-based remote sensing system, the Philippine Government, thru the Department of Science and Technology, in partnership with the University of the Philippines, Japan's Hokkaido University and Tohoku University has launched a satellite system research project known as the Philippine Scientific Earth Observation Micro-Satellite (PHL-Microsat) Program. It's the first research project of the Philippine government which aims to launch the country's first Filipino-assembled microsatellites Diwata-1 and Diwata-2 by Year 2016 and 2017. Equipped with remote-sensing sensors, it seeks to maximize and utilize earth observation capabilities as applied in resource and disaster management and weather observations through multispectral images taken by its cameras. In April 2016, Diwata-1 has been successfully launched into space.

2. Importance

Diwata-1 contains three payloads: a high-precision telescope, a wide-range field camera and a space-borne multispectral imager which uses a Liquid Crystal Tunable Filter. Its optical systems has been manufactured and assembled especially for its mission. The optical imaging sensors contain   radiometric noise and geometric distortions that needs to be examined and corrected. To increase the accuracy and precision of the information from

the images produced, they need to undergo standard corrections and processes which needs to be developed. Further projection unto real-world coordinates is necessary to produce level 1 satellite images that can be used or processed by government agencies and research institutions for a wide-range of possible applications.

3. Limitations

This research will discuss the pre-launch calibration research done for Diwata-1 with emphasis on the parameter determination for the CCD+Optics Correction and geometric distortions elimination. The researchers used data from laboratory and practical airborne experiments of an LCTF Camera to design the image-processing line. Corrections introduced include radiance offsets, reduction of transmittance limitation and vignetting caused by the camera's optical assembly composed of a charge-coupled device (CCD), filter and lenses. The laboratory experiment was done in Japan while the practical airborne experiment was done in the Philippines, both used the same LCTF Camera.

PERFORMANCE EXPERIMENTS

1. Laboratory Experiment

This laboratory experiment was done in Hokkaido University. The objective of the activities was to obtain initial calibration constant that converts digital numbers to radiance. An integrating sphere was used to allow an environment with uniform spectral radiance. The calibration constant was given by:

$$C(\lambda) = \frac{L(\lambda)}{DN * exposure\ time}$$
(1)

Where : $C(\lambda)$ = Calibration coefficient
$L(\lambda)$ = spectral radiance value
DN = digital number or pixel value

Noting that the calibration constants also varies linearly with the gain value, the researchers took images with the LCTF Camera in different exposure time and gain values. Images were taken inside the integrating sphere where radiance must also be uniform.
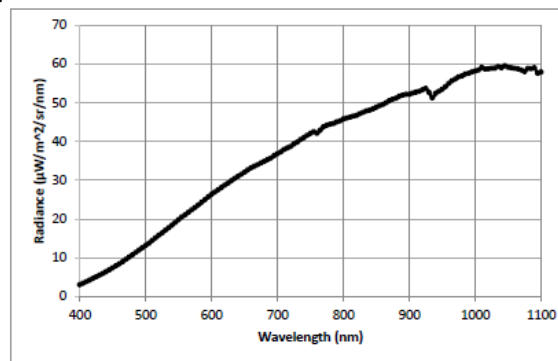

Figure 1. Spectral Radiance inside the Integrating Sphere

2. Practical Airborne Experiment

The practical airborne experiment was done in the towns of Catarman, Samar and Gerona, Tarlac, both in the Philippines, last August 2015 and March 2016. The LCTF camera was mounted onto a Cessna Plane, together with an Compact Airborne Spectrographic Imager (CASI), hover above preselected agricultural areas around the locations. As the LCTF and CASI capture images, ground teams simultaneously acquired spectral signatures of the target vegetation to serve as reference values. In the Catarman Campaign, an Ocean Optics USB4000 Spectrometer was used while an ASD Spectroradiometer was utilized during the Tarlac Campaign.
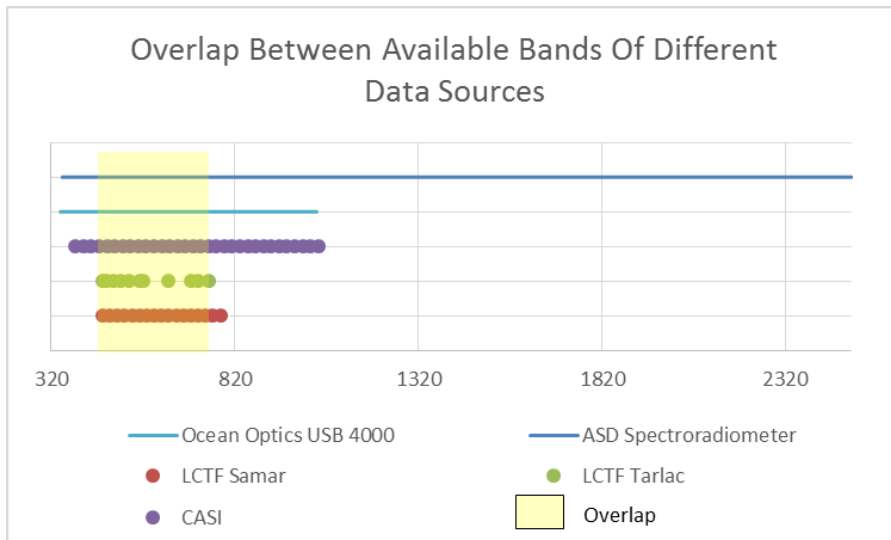
Figure 2. Overlap Between the Bands Collected by Various Sensors

In the Catarman Campaign, the LCTF captured 17 bands with a 0.8 millisecond exposure time each over areas of rice field, mangroves and river. In the Tarlac Campaign, the number of bands was narrowed down to 11 to allow greater overlaps among the images and considering the bands crucial to land observation, vegetation management and ocean color monitoring.
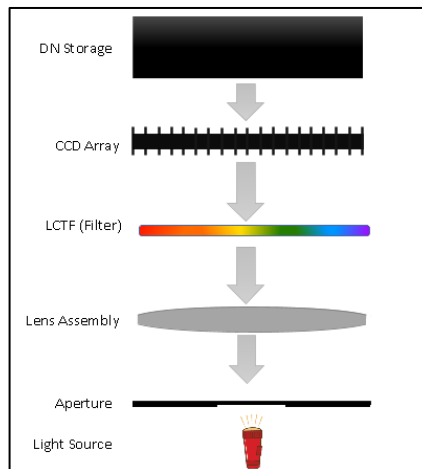
RESULTS AND DISCUSSION

1. CCD Optics Correction

Figure 3. LCTF Camera Optical Assembly

The figure above shows an illustration of the LCTF Camera's Optical Assembly. As the light enters the system, it passes through different layers. Each introduces a correction to the images. It was examined using the images from the laboratory experiment.
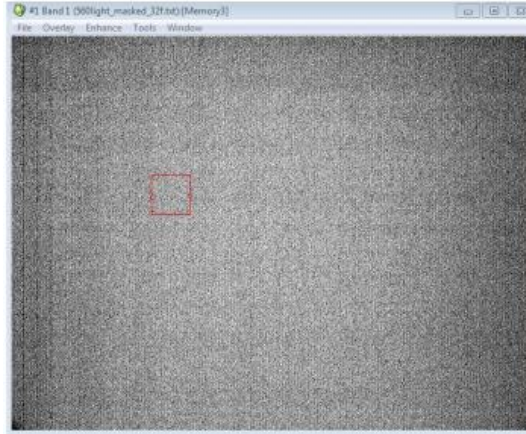
Figure 4. Integrating Sphere Image at 560 nm (viewed thru ENVI)

The calibration constants derived from the laboratory experiment to convert DN to radiance was applied first in the raw pixel values. To reduce the transmittance limitation of the filter and the correction introduced by the lens assembly, the following formula was produced:

$$E_\lambda = DN * C_\lambda * \tau_\lambda * LensCorr_\lambda(x,y) \qquad (2)$$

where: E_λ = irradiance at the integrating sphere
DN = Pixel Value in DN
C_λ = calibration constant at specific band
τ_λ = Filter Factor
$LensCorr_\lambda (x,y) = r*k_1 + k_2$
r = radius from the image center (in pixel)
k_1, k_2 = lens correction parameters
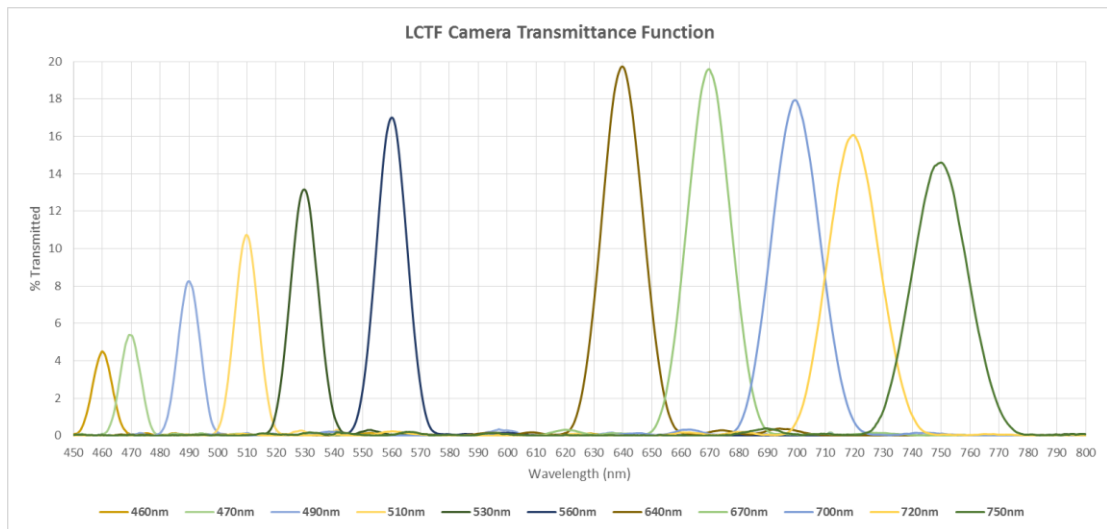
1.1 Filter Correction

Figure 5. Transmittance Function of the LCTF Camera

The figure above shows the transmittance limitation of the LCTF Camera at the 11 preselected bands. This shows that at most, only around 20% of the total transmittance could be recorded by the LCTF Camera. Mathematical computations must be computed to get the 100% transmitted energy given the following equation:

$$100\% Transmitted_\lambda = DN * \tau_\lambda \qquad (3)$$

To get the filter factor for each band, we use:

$$\tau_\lambda = \frac{\int_{\lambda 1}^{\lambda 2} 100\% Transmitted(\lambda)}{\int_{\lambda 1}^{\lambda 2} Actual\% Transmitted(\lambda)} \tag{4}$$

Bandwidth for each central wavelength of each band is different. Wavelength boundaries are selected removing the data from the noisy regions.

λ	τ
460nm	56.75424062
470nm	25.61521501
490nm	18.37355722
510nm	16.7230301
530nm	23.1279274
560nm	13.2770684
640nm	11.32679694
670nm	11.04921552
700nm	12.29805613
720nm	14.07537742
750nm	18.07885111

Table 1. Computed Filter Factor for each band.

Table 1 shows the filter factor computed for each of the 11 wavelengths. Given these values, the only unknown in eq (2) is the lens correction parameters k1 and k2.

1.2 *Lens Assembly Correction*

As the light enters the lens assembly, another correction caused by the energy loss along the refraction of light was introduced. To determine how to minimize this error, the behavior and trend of DN values across the pixels of each images were examined.
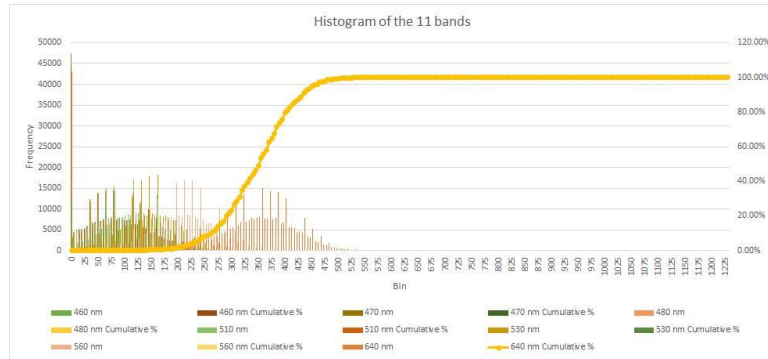

Figure 5. Histogram of Pixel Values along

As seen in Figure 5, DN values of the integrating sphere images are not normally distributed. In determining the lens correction parameters, a simple median filter was applied to remove noisy data.
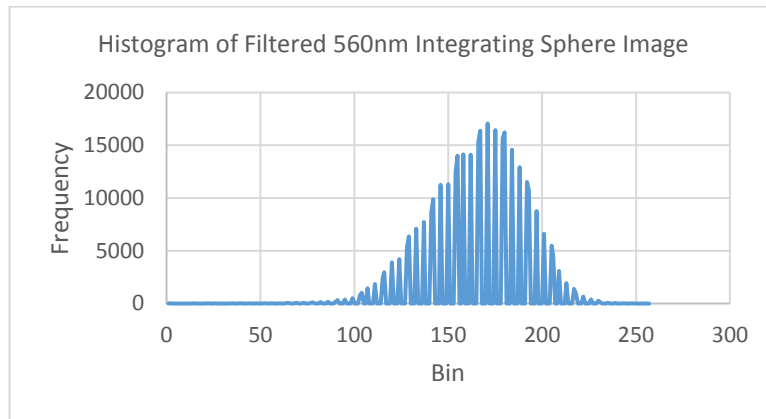
Figure 6. Histogram of Filtered 560nm Integrating Sphere Image

Figure 6 shows the data for the median filtered 560nm integrating sphere image. The Distribution curve has been normalize. This result was also found in the other 10 integrating sphere images.
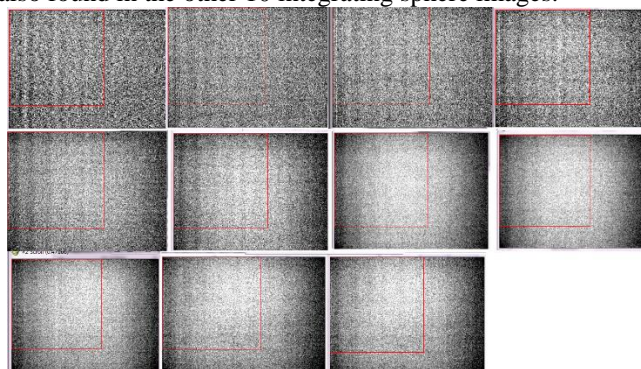

Figure 7. Median Filtered Integrating Sphere Images (1st row L-R: 460nm, 470nm, 490nm, 510nm | 2nd row, L-R: 530nm, 560nm, 640nm | 3rd row L-R: 670nm, 700nm, 720nm, 750nm)

Looking into the integrating sphere images in Figure 7, a radial pattern originating from the image center was observed resulting to the assumption of the equation below:

$$\text{LensCorr}_\lambda\,(x,y) = r*k_1 + k_2 \tag{5}$$

Where: r = radius from the image center (in pixel)
         k_1, k_2 = lens correction parameters

To determine k1 and k2 constants for equation (5), a least squares method was used. A total of 11 matrix equations were calculated to determine the k values for each band.

	K1(multiplicative)	K2(additive)
460 nm	0.000004228	0.002341
470 nm	0.00001033	0.005238
480 nm	0.00001275	0.006513
510 nm	0.00001275	0.006513
530 nm	0.00001048	0.00004574
560 nm	0.00001681	0.007727
640 nm	0.00001159	0.007365
670 nm	0.00001015	0.006513
700 nm	0.000006577	0.004541

720 nm	0.000004577	0.003157
750 nm	0.000003675	0.00215

Table 2. Summary of Computed Lens Correction Parameters.

Upon determination of the filter factor and lens correction parameters, equation 2 has been applied to each pixel of the 11 raw integrating sphere images. Raw and corrected values were compared to their corresponding ideal values.
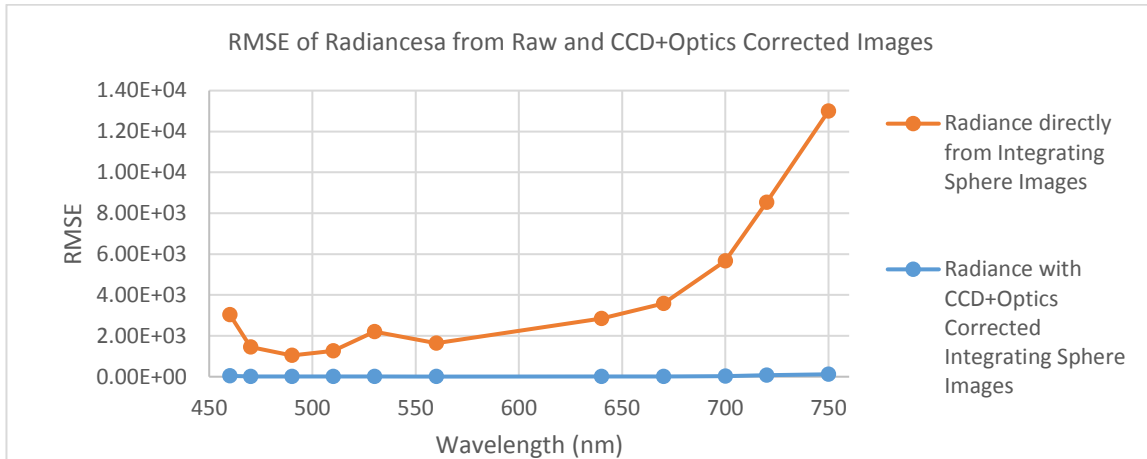

Figure 8. RMSE with standard deviation plots of raw and CCD + Optics Corrected Integrating Sphere Images

The RMSE of processed images went down by at most 3568.5 µw/m2/sr/nm and improved by 98.76% to 99.76%. Correction introduced was effective across all the 11 bands.

Figure 9. (L-R) Raw LCTF image CCD+Optics corrected image
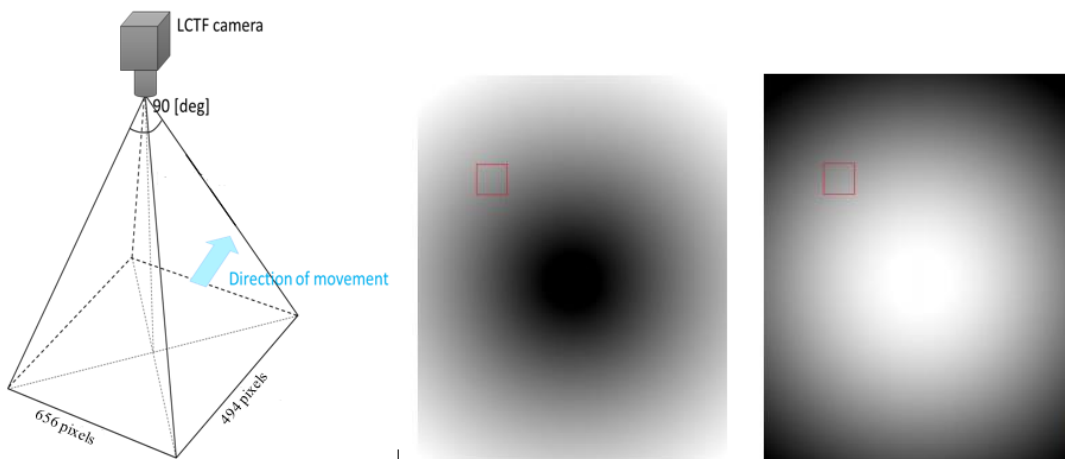
2. *Field-of-View Correction*

Figure 10. (L-R) Visualization of the LCTF Fielf of View, Correction Image θ and Correction Image Cos(θ)

The field of view angle correction accounts for the differences of the path traveled by the irradiance on the surface before it reaches the sensor. As the surface gets farther from the optical center, it travels a longer path and energy lost is greater. To eliminate this variation across the image, a field-of-view correction described below is introduced:

$$DN_{FOV\text{-}corrected} = DN/\cos(\theta) \tag{6}$$

where: $DN_{FOV\text{-}corrected}$ = FOV-corrected DN value
Θ = angle between the optical axis and the line connecting the optical center and the surface

3. *Radial-Lens Distortion Correction*

Figure 11. (L-R) Raw LCTF Image and Radial-Lens Corrected LCTF Image

Radial lens distortion is an optical correction present in all raw images captured from a frame camera. A technical report prepared by Zhengyou Zhang entitled "A Flexible New Technique for Camera Calibration" discusses a way to correct this. Intrinsic parameters and distortion coefficients was determined and used in a developed python code.

4. *Georeferencing*

Figure 12. Georeferenced LCTF Image

Georeferencing of the LCTF images was done manually by an ENVI Software. The sample georeferenced LCTF images above used Universal Transverse Mercator Zone 51 North ans WGS-84 datum.

5. *Sun-Angle Correction*

The position of your light source also affects the data from the images. Thus, the direction of the sun during the time of acquisition must also be taken into account.

$$DN_{Sun\text{-}AngleCorrected} = DN / (\sin\Phi\sin\delta + \cos\Phi\cos\delta\cos\omega) \tag{7}$$

where: $DN_{Sun\text{-}AngleCorrected}$ = Sun-Angle Corrected DN Values

$$\Phi =$$
$$\delta =$$
$$\omega =$$

An equation, described in equation (7) was derived from the Simple Solar Spectral Model developed by R. Bird and C. Riordan was used to account for the corrections. Using the time of acquisition and coordinate of the target areas, the solar positions were determined.
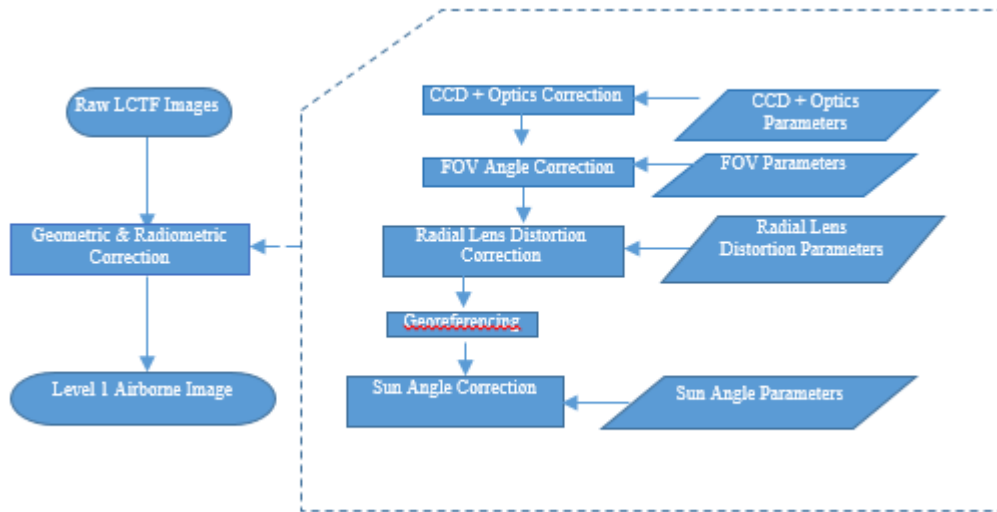
6. *Standard Methodology Developed*

Figure 13. Methodology established for the airborne images

The methodology produced was based on the determined possible sources of error and to answer the need to produce images more precise and usable satellite images. All correction parameters and methodology was applied to the data gathered from the April 1 Morning and April 2 Afternoon flights of the Airborne Campaign in Catarman. The processed data was then compared to the radiance data acquired through the spectroradiometer.
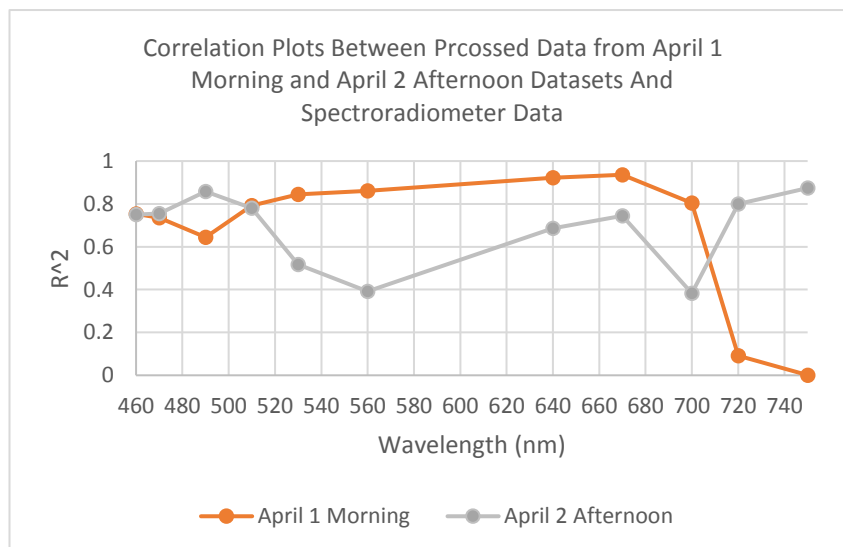

Figure 14. Correlation Plots Between Prcossed Data from April 1 Morning and April 2 Afternoon Datasets And Spectroradiometer Data

The correlation values between the April 1 Morning Dataset and the spectroradiometer data ranges from 0.001 to 0.9361. That of the April 2 Afternoon dataset ranges from 0.3831 to 0.8742.
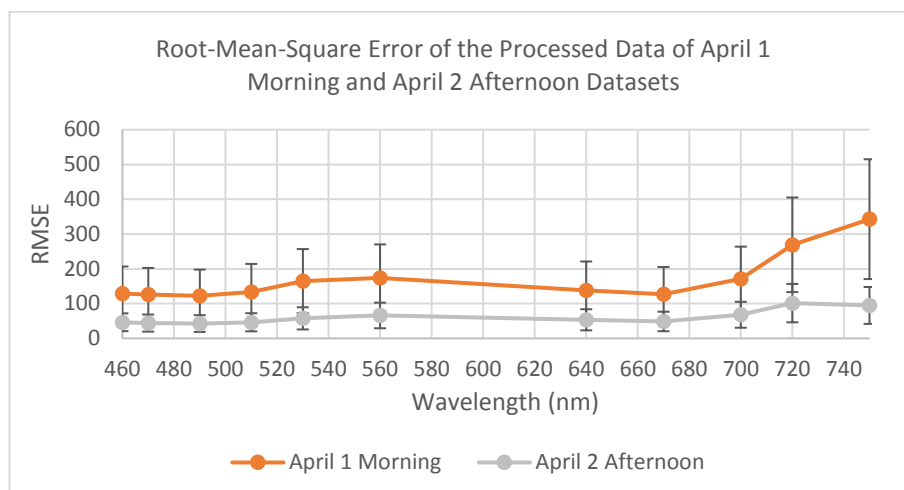
Figure 15. Root-Mean-Square Error of the Processed Data of April 1 Morning and April 2 Afternoon Datasets

For the April 1 Morning Data, the root-mean-square error ranges from 122.3952 µw/m^2/sr/nm to 342.7954 µw/m^2/sr/nm while that of the April 2 Afternoon data ranges from 42.69058 µw/m^2/sr/nm to 101.4406 µw/m^2/sr/nm. Standard deviation is largest on 750 nm band.

CONCLUSION AND RECOMMENDATION

CCD + Optics Correction gave a notable development on the precision of radiance values improving the data by 98.76% at the minimum.Radiometric procedures applied has been proven to increase the reliability amongst data. The vignette-effect was removed. Geometric correction procedures developed effectively reduced the distortion and yields usable level 1 airborne imageries. However, the inconsistency of the results between the two datasets as shown in figures 14 and 15 should be further examined. The standard deviation, and the inconsistency between the two correlations at 750 nm are consistently high. The LCTF Camera behaves badly on this region.

For further research, a post processing determination of calibration coefficients may be introduced to improve the results. The correction procedures must be applied to the rest of the airborne images to strengthen results.

REFERENCES

[1]Bird, R., Riordan, C., December 1984. Simple Solar Spectral Model for Direct and Diffuse Irradiance on Horizontal and Tilted Planes at the Earth's Surface for Cloudless Atmospheres
[2] Kurihara, J., Ishida T.,, Magallon B.,, Vergel K.,, 2015. Diwata's Payload Calibration
[3] Camera Calibration and 3D Reconstruction. retrieved December 2015 from http://docs.opencv.org/2.4/modules/calib3d/doc/camera_calibration_and_3d_reconstruction.html#calibratecamera
[4] Zhang. Z., 1998. A Flexible New Technique for Camera Calibration